POLITECNICO DI TORINO
Repository ISTITUZIONALE

Carbon Nanotube Interconnects: Process Variation via Polynomial Chaos

Original
Carbon Nanotube Interconnects: Process Variation via Polynomial Chaos / Stievano, IGOR SIMONE; Manfredi, Paolo; Canavero, Flavio. - In: IEEE TRANSACTIONS ON ELECTROMAGNETIC COMPATIBILITY. - ISSN 0018-9375. - STAMPA. - 54:1(2012), pp. 140-148. [10.1109/TEMC.2011.2171490]

Availability:
This version is available at: 11583/2458384 since:

Publisher:
IEEE

Published
DOI:10.1109/TEMC.2011.2171490

Terms of use:

This article is made available under terms and conditions as specified in the corresponding bibliographic description in the repository

Publisher copyright

(Article begins on next page)

12 October 2024

Carbon Nanotube Interconnects: Process Variation via Polynomial Chaos

Igor S. Stievano, *Senior Member, IEEE* Paolo Manfredi, *Student Member, IEEE,*
Flavio G. Canavero, *Fellow, IEEE,*

This paper has been submitted for possible inclusion in the Special Issue Issue on Applications of Nanotechnology in Electromagnetic Compatibility (nano-EMC)

***Abstract*—This paper addresses the generation of an enhanced stochastic model of a carbon nanotube interconnect including the effects of process variation. The proposed approach is based on the expansion of the constitutive relations of state-of-the-art deterministic models of nanointerconnects with uncertain parameters in terms of orthogonal polynomials. The method offers comparable accuracy and improved efficiency with respect to conventional methods like Monte Carlo in predicting the statistical behavior of the electrical performance of next generation data links. An application example involving both the frequency- and time-domain analysis of a realistic nanointerconnect concludes this paper.**

***Index Terms*—EMC, Transmission line, Stochastic analysis, Tolerance analysis, Uncertainty, Circuit modeling, Circuit Simulation, Polynomial Chaos, Carbon Nanotubes.**

I. Introduction

Today we find ourselves on the verge of a transition between the traditional copper interconnects and new structures for the high-speed data communication links in next generation devices. Copper interconnects in the nanoscale range suffer from a large resistivity and poor current density and demand for the availability of alternative materials and technological solutions. In recent years, carbon nanotubes (CNT) have been considered good candidates for replacements in future applications due to their impressive mechanical and electrical properties [1]–[5].

In order to reduce the intrinsic highly resistive behavior of a single conductor, carbon nanotube interconnects usually consist of either bundles of numerous single-walled CNTs (SWCNTs, i.e., formed by a mono-atomic layer of graphite) or several graphene sheets arranged in coaxial configuration (multi-walled CNTs, or MWCNTs). In both cases the conductors are usually parallel connected at both ends and excited in common-mode configuration.

Numerical models of CNT interconnects are required for assessing strengths and limitations of application designs implementing this technology. The recent literature proposed a number of models for the description of the electromagnetic behavior of CNT structures. Without loss of generality, we limit ourselves to the results based on the approximation of signal propagation on nanointerconnects via the well-known telegraph equations (e.g., see [6]–[11] and references therein). This class of models allows to simulate realistic nanointerconnects in either the frequency or time domain via conventional transmission-line theory techniques [12]. However, the main limitation of the available approaches is that the proposed CNT models are deterministic, i.e., they describe a nanostructure with predefined values of its electrical and geometrical parameters. As process technology continues to scale downward and physical interconnect dimensions become smaller, the impact of process variations on interconnect characteristics has become increasingly significant and needs to be taken into account. Pioneering work providing a thorough review and discussion on the effects of process variations on the performances of CNT interconnects has been carried out in [13]–[15], though based on a conventional Monte Carlo (MC) approach.

The aim of this paper is the extension of the state-of-the-art transmission line models of a CNT interconnect to account for the inherent variability of model parameters. The advocated method is based on the so-called Polynomial Chaos (PC) theory[1], that assumes a series of orthogonal polynomials of random variables for the solution of a stochastic problem [17]. This technique turns out to be much faster than alternate available solutions for variability, like the aforementioned MC simulation, while maintaining comparable accuracy. It has been successfully applied to several problems in different domains, including the extension of the classical circuit analysis tools, like the modified nodal analysis (MNA), to the prediction of the stochastic behavior of circuits [18]. Recently, these results have been extended to long distributed interconnects described by multiconductor transmission line equations [19]–[20].

II. Multiconductor Transmission Line Model for CNT Interconnects

The basic building structure of a CNT interconnect is represented by a SWCNT. A SWCNT has a diameter on the order of few nanometers and can exhibit either a semiconducting or a metallic behavior depending on the way it is rolled-up.

The interconnect is obtained by the parallel connection of a bundle of SWCNTs as shown in the cross-section of Fig. 1.

Igor Stievano, Paolo Manfredi and Flavio Canavero are with Dipartimento di Elettronica, Politecnico di Torino, 10129 Torino, Italy (e-mail: {igor.stievano,paolo.manfredi,flavio.canavero}@polito.it).

[1]In this context, the word Chaos is used in the sense originally defined by Wiener [16] as an approximation of a Gaussian random process by means of Hermite polynomials.

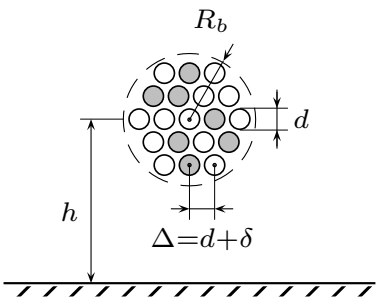

Fig. 1. Cross-section of a typical nanointerconnect composed of a bundle of SWCNTs in horizontal configuration, above the ground plane. The gray circles correspond to the conducting nanotubes.

TABLE I
TYPICAL VALUES AND RANGES OF VARIATIONS FOR PARAMETERS IN FIG. 1.

Variable	Typical value	3σ relative standard deviation
h	~ 100 nm	32%
R_b	~ 10 nm	32%
d	~ 1 nm	50%
δ	~ 0.34 nm	23%

In this structure, h is the height above the ground plane, R_b is the radius of the entire bundle, d is the average diameter of CNTs and δ is the inter-tube distance. For the sake of simplicity, all the nanotubes in the bundle are assumed to have the same average diameter d. This assumption is justified by the typically small variations of the diameter among nanotubes in the same bundle (e.g., 4.4% as reported in [14]). Typical values and ranges of variation for these parameters have been selected according to [10], [14] and are summarized in Tab. I. It is also relevant to remark that approximately one third of the nanotunes in the bundle (represented by the gray circles in Fig. 1) exhibits a purely metallic behavior.

As already outlined in the introduction, an alternative configuration is represented by MWCNTs (see Fig. 2), whose overall radius can reach tens of nanometers. For both the case of bundles of SWCNTs and MWCNTs, equivalent circuits based on multiconductor transmission line theory are available in the literature. As an example, Fig. 3 shows the muticonductor equivalent of a typical single-ended data link base on SWCNTs. Additional details on the model structures are given in the next two subsections.

A. MTL Model for SWCNTs

This Section briefly provides an overview of the available results for the modeling of the signal propagation on the bundle of Fig. 1. A detailed discussion of model derivation can be found in [6], while [11] extends the model to the inclusion of the effects of wrapping and twisting inside the bundle.

Under specific conditions, a SWCNT bundle above a ground plane behaves as an RLC multiconductor transmission line (see Fig. 3, where n_c denotes the number of metallic nanotubes) with a suitable definition of the per-unit-length parameters

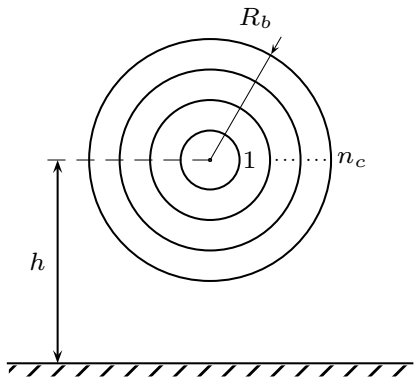

Fig. 2. Cross-section of a MWCNT interconnect above the ground plane.

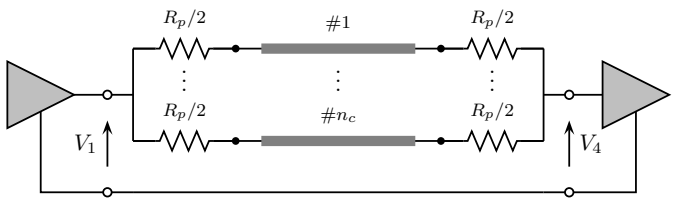

Fig. 3. Multiconductor model of the SWCNT bundle of Fig. 1. This scheme represents the typical configuration of a nanointerconnect used as an high-speed link between a driver and a receiver.

$$\begin{cases} \dfrac{d}{dz}\mathbf{V}(z,s) &= -\left[\mathbf{R}' + s(\mathbf{L}_e + \mathbf{L}_k)\right]\mathbf{I}(z,s) \\ \dfrac{d}{dz}\mathbf{I}(z,s) &= -s(\mathbf{C}_e^{-1} + \mathbf{C}_q^{-1})^{-1}\mathbf{V}(z,s). \end{cases} \tag{1}$$

Specifically, both the inductance and the capacitance matrices of the line are made of two contributions. The classical magnetic inductance matrix ($\mathbf{L}_e$) and electrostatic capacitance matrix ($\mathbf{C}_e$), which are full and can be computed via standard analytical formulas or numerical methods, are combined with two new diagonal matrices, namely the so-called *kinetic inductance* matrix $\mathbf{L}_k$ and *quantum capacitance* matrix $\mathbf{C}_q$, whose entries are given by

$$L_{k,ii} = \frac{h}{8e^2\nu_F}, \quad C_{q,ii} = \frac{8e^2}{h\nu_F}, \tag{2}$$

where $h = 6.626 \times 10^{34}$ Js is the Plank constant, $e = 1.602 \times 10^{19}$ C is the single electron charge and ν_F is the *Fermi velocity*; moreover, the number of conducting channels in a metallic nanotube is assumed to be equal to 2, although more accurate formulae could be used [7]–[8]. For the case of graphene, $\nu_F \approx 8 \times 10^5$ m/s and the above parameters become $L_{k,ii} = 4\,\mathrm{nH}/\mu\mathrm{m}$ and $C_{q,ii} = 0.4$ aF/nm. Losses are described by the per-unit-length matrix $\mathbf{R}'$, which is also diagonal, and by two identical lumped series resistors $R_p/2$ on each conductor, that are independent of the line length and account for the intrinsic quantum resistance of a nanotube. The above parameters write

$$R_p = h/4e^2, \quad R'_{ii} = R_p/\lambda_{\mathrm{mfp}}, \tag{3}$$

where $\lambda_{\rm mfp}$ is the *mean-free-path* of free electrons. In the low bias condition, i.e., for a longitudinal electric field less than $0.16\,$V/m, it is on the order of $1\,\mu$m. The intrinsic resistance is $R_p = 6.45\,\mathrm{k}\Omega$.

B. MTL Model for MWCNTs

A similar model can also be derived for MWCNT interconnects, whose cross-section is depicted in Fig. 2 [7]–[9]. This alternative configuration leads to a multiconductor model similar to that in Fig. 3, where the conductors correspond to the different shells of the MWCNT structure. Again, the wave propagation can be described by means of (1), where the p.u.l. quantum parameters $L_{k,ii}$, $C_{q,ii}$ and R'_{ii} take the same form as in (2) and (3), whereas $\mathbf{L}_e$ and $\mathbf{C}_e$ are computed with classical analytical formulae for multiple coaxial structures.

III. Equivalent Single Conductor Model

Since the nanotubes are short-circuited at both ends and excited in common-mode configuration, it is possible to derive an equivalent single-conductor transmission-line model like the one shown in Fig. 4, characterized by the scalar p.u.l. parameters R', L_k, L_e, C_q, C_e [8], [10]. This simplified model unavoidably introduces some approximations but it is much simpler than the one of Fig. 3 and requires less information for the computation of model parameters.

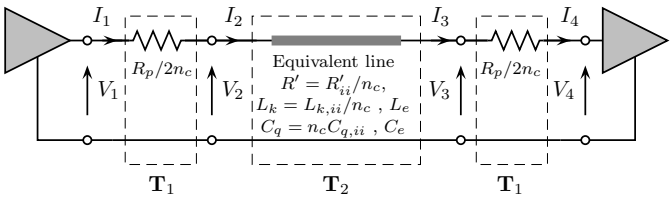

Fig. 4. Single-conductor equivalent transmission-line model of a CNT interconnect.

The underlying hypothesis is that identical currents flow into the different terminals of the multiconductor transmission line of Fig. 3. Owing to this, for both a SWCNT bundle and a MWCNT the p.u.l. resistance and the kinetic inductance turn out to be weighted by the actual number of conductive CNTs n_c, i.e.,

$$R' = \frac{R'_{ii}}{n_c} = \frac{h}{8n_c e^2 \lambda_{\rm mfp}}, \quad L_k = \frac{L_{k,ii}}{n_c} = \frac{h}{8n_c e^2 \nu_F}. \tag{4}$$

The quantum capacitance is $C_q = n_c C_{q,ii}$ for the SWCNT bundle, and

$$C_q = \alpha n_c + \beta r_1 + \gamma \tag{5}$$

for the MWCNT case [8]. In the latter equation r_1 is the inner shell radius expressed in nanometers, $\alpha = 2.56 \times 10^{-2}$ nF/m, $\beta = 7.525 \times 10^{-2}$ F/m^2 and $\gamma = 9.887 \times 10^{-2}$ nF/m. Nevertheless, for structures consisting of a relatively small number of CNTs, the magnetic inductance and the quantum capacitance can be neglected, leading to a model that is even simpler.

It is worth noticing that the classical p.u.l. parameters for the structures of Fig. 1 and Fig. 2 are computed by considering the geometrical parameters defining the external shape of the cross-sections, i.e., the radius R_b and the eight h. In turn, the electrostatic capacitance and magnetic inductance write:

$$C_e = 2\pi\epsilon_0/\cosh^{-1}(h/R_b), \quad L_e = \mu_0\varepsilon_0 C_e^{-1}. \tag{6}$$

In the case of a SWCNT bundle, the radius R_b can be easily computed by assuming a regular distribution of the nanotubes arranged in a predefined geometrical shape (e.g., an hexagon). In this case, simple analytical formulae can be used, as suggested in [10]:

$$R_b = a + \Delta(N_s - 1), \tag{7}$$

where $\Delta = 2a + \delta$ and N_s is the number of SWCNTs constituting the external side of the hexagon, that is related to the total number of nanotubes N_c by

$$N_c = 1 + \sum_{i=1}^{N_s} 6(i-1); \tag{8}$$

in this study, the intertube distance δ is assumed to be $0.34\,$nm.

It is important to remark that the scheme of Fig. 4 can be further improved by including the effects of the nonideal metallic contacts of the nanotube. This can be easily done by means of two lumped series resistors with values depending on the manufacturing process. Without loss of generality, the above contact resistances are neglected in the test cases considered in this study.

IV. Impact of Process Variation

A detailed discussion of the technological aspects impacting the electrical performance of nanotube interconnects is out of the scope of this paper. Reference [14] provides a useful overview aimed at (i) identifying the potential sources of variation on SWCNT bundle interconnects based on the structure of Fig. 1, (ii) quantifying the expected statistical distribution of each type of variation based on current experimental results, and (iii) calculating the relative impact of each source of variation on the model parameters and on the electrical performance of the interconnect, thus highlighting the variations that will be important for future nanotube bundle-based interconnect solutions.

Among the different sources of variations, in this paper we select and focus on three parameters that have been demonstrated to be major sources of uncertainty with a large impact on the interconnect performance. Namely, the number of conducting nanotubes, the height of the bundle over the ground plane and the diameter of a single nanotube.

As outlined in Sec. II, a nanotube bundle like the one of Fig. 1 is composed by n_c conducting nanotubes, where n_c is approximately one third of the total number N_c. More precisely, if a nanotube has a probability r=1/3 to behave as a metallic conductor, the probability density function of the discrete variable n_c is the binomial distribution. However, when the total number of conductors is large enough (and this always occurs in practice), the binomial distribution can be

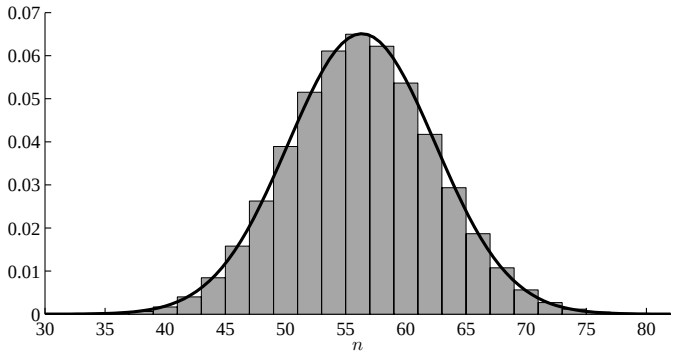

Fig. 5. Binomial probability function (bars) and its approximation via a Gaussian distribution (continuous thick line). The two probability plots are obtained for a total number of nanotubes $N_c = 169$ and for a probability $r = 1/3$ of conduction.

effectively approximated by the continuous normal distribution with expected value rN_c and variance $rN_c(1-r)$ (see Fig. 5). Also, as suggested in [14], the two remaining uncertain parameters, i.e., the height h and diameter d of Fig. 1, can be effectively represented by Gaussian random variables.

Based on the above discussion, the three selected parameters write

$$\begin{cases} n_c = \bar{n}_c(1+\sigma_n\xi_1) \\ h = \bar{h}(1+\sigma_h\xi_2) \\ d = \bar{d}(1+\sigma_d\xi_3), \end{cases} \tag{9}$$

where ξ_1, ξ_2 and ξ_3 are independent random variables with standard normal distribution (i.e., with zero mean and unit variance), $\bar{n}_c$, $\bar{h}$, $\bar{d}$ are the mean values of the parameters and the σ coefficients are their corresponding normalized standard deviations.

It is relevant to remark that the three normalized distributions are assumed to be statistically independent even if some correlation among the parameters may exists (e.g., see [21]). This information, however, can be taken into account a-posteriori since the proposed PC method allows for the generation of an extended model of a circuit element and of its response expressed in terms of a known parametric function of the uncertain quantities. When the correlation among the random parameters is known and available, the statistical information of the system response (e.g., expressed in terms of its probability distribution) can be computed from the advocated parametric response by exploiting this information.

V. Stochastic Simulation of Nanointerconnects

This Section summarizes the proposed procedure for the stochastic simulation of a nanointerconnect that is described by either the full MTL model of Fig. 3 or the simplified equivalent of Fig. 4.

For the sake of clarity and simplification, the formal development of our discussion is based on the ESC model. Some additional details on the extension to the MTL model will be given later on.

The proposed strategy is the following: (i) generate extended stochastic models of the different parts composing the cascaded structure that will be able to include the effects of the statistical variation of model parameters, i.e., of the stochastic parameter defined by (9), and (ii) simulate the entire structure in the frequency-domain by suitably concatenating these models.

In this study, the different cascaded blocks are represented in terms of their transmission matrix in the Laplace domain. The transient response is achieved by harmonic superposition. Finally, the source and load elements of Fig. 4 are assumed to be described by linear Thevenin equivalents.

A. Model of Lumped Blocks.

The two-port identical lumped elements defined by the series resistors of Fig. 4 are represented by their transmission matrix $\mathbf{T}_1$. As an example, in the absence of parameter uncertainty, the electrical law governing the block on the left writes

$$\underbrace{\begin{bmatrix} V_2 \\ I_2 \end{bmatrix}}_{\mathbf{X}_2} = \underbrace{\begin{bmatrix} T_{1,11} & T_{1,12} \\ T_{1,21} & T_{1,22} \end{bmatrix}}_{\mathbf{T}_1} \underbrace{\begin{bmatrix} V_1 \\ I_1 \end{bmatrix}}_{\mathbf{X}_1} = \begin{bmatrix} 1 & -R_p/2n_c \\ 0 & 1 \end{bmatrix} \mathbf{X}_1; \tag{10}$$

the same relation involving the port vectors $\mathbf{X}_4$ and $\mathbf{X}_3$ is used to represent the lumped block on the right.

When the problem becomes stochastic, with some random parameters expressed as in (9), we must consider the entries of (10) as random quantities. In turn, (10) becomes a stochastic equation leading to randomly-varying voltages and currents:

$$\mathbf{X}_2(\boldsymbol{\xi}) = \mathbf{T}_1(\boldsymbol{\xi})\mathbf{X}_1(\boldsymbol{\xi}), \tag{11}$$

where vector $\boldsymbol{\xi}$ collects the random variables ξ_i which the system depends on.

PC is a powerful tool allowing to solve in a clever way stochastic equations [17]. The idea behind this technique is the approximation of a random variable in terms of a truncated series of orthogonal polynomials that are functions of a predefined standard distribution. As a clarifying analogy, we can think of these polynomials as the sinusoidal functions in the Fourier series expansion. As an example, for the case of Gaussian random variables, the univariate orthogonal basis functions are the Hermite polynomials $\phi_0{=}1$, $\phi_1{=}\xi_1$, $\phi_2{=}(\xi_1^2-1)$,.... When dealing with multiple random variables, these basis functions are replaced by a product combination – that preserves orthogonality – of univariate polynomials, thus leading to a multivariate version of the Hermite polynomials, as exemplified in Tab. II for three random variables.

For the current application, both the voltage and current variables of (11) as well as the matrix $\mathbf{T}_1$, can be represented in terms of a truncated series. For instance, the second-order expansion of the element 21 of matrix $\mathbf{T}_1$ with $\bar{n}_c = 60$ and $\sigma_n = 0.1$ writes

$$T_{1,21}(\boldsymbol{\xi}) = -\frac{R_p}{2n_c} = -\frac{R_p}{2\bar{n}_c(1+\sigma_n\xi_1)} \approx -\frac{R_p}{2}\cdot$$
$$\cdot\left(1.68\,10^{-2}\phi_0(\boldsymbol{\xi}) - 1.73\,10^{-3}\phi_1(\boldsymbol{\xi}) + 1.77\,10^{-4}\phi_4(\boldsymbol{\xi})\right), \tag{12}$$

TABLE II
HERMITE POLYNOMIALS FOR THE CASE OF THREE RANDOM VARIABLES ($n = 3$, $\boldsymbol{\xi} = [\xi_1, \xi_2, \xi_3]^T$) AND A SECOND ORDER EXPANSION ($p = 2$).

index k	order p	k-th basis ϕ_k	$< \phi_k^2 >$
0	0	1	1
1	1	ξ_1	1
2	1	ξ_2	1
3	1	ξ_3	1
4	2	$\xi_1^2 - 1$	2
5	2	$\xi_1\xi_2$	1
6	2	$\xi_1\xi_3$	1
7	2	$\xi_2^2 - 1$	2
8	2	$\xi_2\xi_3$	1
9	2	$\xi_3^2 - 1$	2

TABLE III
HERMITE POLYNOMIAL CHAOS DEFINITIONS AND PROPERTIES.

Object	e.g., network function or parameter $\mathbf{T}(\boldsymbol{\xi})$ that depends on $\boldsymbol{\xi} = [\xi_1, \xi_2, \ldots, \xi_n]^T$
Expansion	$\mathbf{T}(\boldsymbol{\xi}) = \sum_{k=0}^{P} \mathbf{T}_k \cdot \phi_k(\boldsymbol{\xi})$
Orthogonal basis	Hermite polynomials $\{\phi_k(\boldsymbol{\xi})\}$ (e.g., see Tab. II for the case $n = 3$)
Number of terms	$P + 1 = (p + n)!/p!n!$
Inner product	$< \phi_k, \phi_j >= \int_{\Re^n} \phi_k(\boldsymbol{\xi})\phi_j(\boldsymbol{\xi})W(\boldsymbol{\xi})d\boldsymbol{\xi}$
Weighting function	$W(\boldsymbol{\xi}) = \frac{1}{\sqrt{(2\pi)^n}} \exp(-\frac{1}{2}\boldsymbol{\xi}^T\boldsymbol{\xi})$
Orthogonality	$< \phi_k, \phi_j >=< \phi_k^2 > \delta_{kj}$
Expansion coefficients	$\mathbf{T}_k =< Y, \phi_k > / < \phi_k^2 >$
Mean	$\mathbf{T}_0$

where the coefficients of the expansion are computed according to the formulas of Table III. It should be noted that some coefficients are zero since in this particular case the element only depends on ξ_1. As a brief summary, we may say that in general the above expansion terms can be computed via the projection of a nonlinear multivariate function of the random variables $\xi_1, \xi_2, \ldots$ onto the orthogonal polynomials ϕ_k. Readers are referred to [18], [22] and references therein for a comprehensive and formal discussion of polynomial chaos application to discrete circuits.

In general, for the matrix $\mathbf{T}_1$, the complete PC expansion writes

$$\mathbf{T}_1(\boldsymbol{\xi}) = \sum_{k=0}^{P} = \mathbf{T}_{1,k}\phi_k(\boldsymbol{\xi}), \tag{13}$$

where $P + 1$ is the total number of terms that generally lies within the range from two to twenty for practical applications and the $\mathbf{T}_{1,k}$ matrices are the expansion matrices.

For a predefined order (e.g., $p = 1$ that means $P = 4$), the use of (13) in (11), along with a similar expansion of the unknown voltage and current variables, yields

$$\begin{aligned} &\mathbf{X}_{2,0}\phi_0(\boldsymbol{\xi}) + \mathbf{X}_{2,1}\phi_1(\boldsymbol{\xi}) + \mathbf{X}_{2,2}\phi_2(\boldsymbol{\xi}) + \mathbf{X}_{2,3}\phi_3(\boldsymbol{\xi}) = \\ &(\mathbf{T}_{1,0}\phi_0(\boldsymbol{\xi}) + \mathbf{T}_{1,1}\phi_1(\boldsymbol{\xi}) + \mathbf{T}_{1,2}\phi_2(\boldsymbol{\xi}) + \mathbf{T}_{1,3}\phi_3(\boldsymbol{\xi})) \cdot \\ &(\mathbf{X}_{1,0}\phi_0(\boldsymbol{\xi}) + \mathbf{X}_{1,1}\phi_1(\boldsymbol{\xi}) + \mathbf{X}_{1,2}\phi_2(\boldsymbol{\xi}) + \mathbf{X}_{1,3}\phi_3(\boldsymbol{\xi})) . \end{aligned} \tag{14}$$

Projection of (14) on the first four Hermite polynomials leads to the following augmented system, where the random variable $\boldsymbol{\xi}$ does not appear, due to projection integral

$$\underbrace{\begin{bmatrix} \tilde{\mathbf{V}}_2 \\ \tilde{\mathbf{I}}_2 \end{bmatrix}}_{\tilde{\mathbf{X}}_2} = \underbrace{\begin{bmatrix} \tilde{\mathbf{T}}_{1,11} & \tilde{\mathbf{T}}_{1,12} \\ \tilde{\mathbf{T}}_{1,21} & \tilde{\mathbf{T}}_{1,22} \end{bmatrix}}_{\tilde{\mathbf{T}}_1} \underbrace{\begin{bmatrix} \tilde{\mathbf{V}}_1 \\ \tilde{\mathbf{I}}_1 \end{bmatrix}}_{\tilde{\mathbf{X}}_1} . \tag{15}$$

According to the above equation, the new vectors $\tilde{\mathbf{V}} = [\mathbf{V}_0, \ldots, \mathbf{V}_3]^T$ and $\tilde{\mathbf{I}} = [\mathbf{I}_0, \ldots, \mathbf{I}_3]^T$ are defined to collect the different coefficients of the polynomial chaos expansion of the unknown voltage and current variables. Each block of $\tilde{\mathbf{T}}_1$ takes the following form

$$\tilde{\mathbf{T}}_{1,ij} = \begin{bmatrix} T_{1,ij,0} & T_{1,ij,1} & T_{1,ij,2} & T_{1,ij,3} \\ T_{1,ij,1} & T_{1,ij,0} & 0 & 0 \\ T_{1,ij,2} & 0 & T_{1,ij,0} & 0 \\ T_{1,ij,3} & 0 & 0 & T_{1,ij,0} \end{bmatrix}, \tag{16}$$

where $T_{1,ij,k}$ denotes block ij of the k-th expansion coefficient of matrix $\mathbf{T}_1$.

It is worth noticing that equation (15) belongs to the same class of (10) and plays the role of the set of equations of a multiterminal circuit element, whose number of terminals is $(P+1)$ times larger than in the original circuit. However, for small values of P (as typically occurs in practice) the additional overhead in handling the augmented equations is much less than the time required to run a large number of MC simulations.

B. Model of Distributed Lines.

Similarly, the extended two-port description of the transmission line can be obtained via the orthogonal projection of the telegraph equations governing the signal propagation along the single equivalent line of Fig. 4. The above projection leads to an extended set of multiconductor transmission line equations, with augmented matrices $\tilde{\mathbf{R}}$, $\tilde{\mathbf{L}}$ and $\tilde{\mathbf{C}}$ that collect the expansion coefficients of the p.u.l. parameters with the same relation as in (16). Readers are referred to [19] and [20] for additional details on the extended model derivation.

The augmented multiconductor equation is then used to generate the transmission matrix defining the extended characteristics $\tilde{\mathbf{T}}_2$ of block $\mathbf{T}_2$ [12]

$$\tilde{\mathbf{X}}_3 = \tilde{\mathbf{T}}_2\tilde{\mathbf{X}}_2 = \mathrm{expm}\left(-\begin{bmatrix} 0 & \tilde{\mathbf{R}} + s\tilde{\mathbf{L}} \\ s\tilde{\mathbf{C}} & 0 \end{bmatrix}\mathcal{L}\right)\tilde{\mathbf{X}}_2, \tag{17}$$

where $\mathcal{L}$ is the line length and the interpretation of the new variables is straightforward.

C. Boundary Conditions and Simulation.

For the deterministic case, the simulation of an interconnect like the one of Fig. 4 amounts to combining the characteristics of the different circuit elements, including the driver and the receiver, and solving the system. This is a standard procedure as illustrated for example in [12] (see Ch.s 4 and 5).

As an example, when a multiport Thevenin equivalent (defined by a voltage source E_S and a series impedance Z_S) and an impedance (Z_L) are used to describe the driver and the receiver of Fig. 4, respectively, the port equations of the terminations in the Laplace domain become

$$\begin{cases} V_1(s) &= E_S(s) - Z_S(s)I_1(s) \\ V_4(s) &= Z_L(s)I_4(s), \end{cases} \tag{18}$$

where the port voltages and currents need to match the equivalent characteristic of the cascade connection of the three blocks $\mathbf{T}_1\mathbf{T}_2\mathbf{T}_1$.

Similarly, when the problem becomes stochastic, the augmented equations (15) and (17) are used in place of the deterministic ones together with the projection of the characteristics of the source and the load elements on the first $(P+1)$ polynomials. It is worth noticing that in this specific example, no variability is included in the terminations and thus the augmented characteristics of the source and load turn out to have a diagonal structure with null contributions of the projection of (18) on the k-th Hermite polynomials, with $k > 0$.

Once the unknown voltages and currents are computed, the quantitative information on the spreading of circuit responses can be readily obtained from the analytical expression of the unknowns. As an example, the frequency-domain solution of the magnitude of voltage V_4 with p=1, leads to

$$\begin{aligned} V_4(j\omega,\boldsymbol{\xi}) = V_{4,0}(j\omega)\phi_0(\boldsymbol{\xi}) + V_{4,1}(j\omega)\phi_1(\boldsymbol{\xi}) + \\ + V_{4,2}(j\omega)\phi_2(\boldsymbol{\xi}) + V_{4,3}(j\omega)\phi_3(\boldsymbol{\xi}). \end{aligned} \tag{19}$$

The above relation is a known nonlinear function of the random variables in $\boldsymbol{\xi}$ that can be used to compute the PDF of $|V_4(j\omega,\boldsymbol{\xi})|$ via standard techniques as numerical simulation or analytical formulas.

D. Time-Domain Solution.

The time-domain response is obtained from the frequency-domain solution by considering a periodic input source and expressing it in terms of a truncated Fourier series

$$e_S(t) \simeq \bar{e}_S + \sum_{m=1}^{M} e_{Sm}\mathrm{e}^{j2\pi f_m t} + e^*_{Sm}\mathrm{e}^{-j2\pi f_m t}, \tag{20}$$

where $\bar{e}_S$ is the signal average over one period and e_{Sm} is the complex Fourier coefficient for the m-th harmonic at frequency f_m. Being the system of Fig. 4 linear, its time-domain behavior is in principle obtainable by the superposition of the analyses carried out for all signal harmonics. For the individual solution at frequency f_m, the voltage source of Fig. 4, appearing also in (18), is replaced by its m-th harmonic component, i.e., $E_S(s_m) = E_S(j2\pi f_m) = e_{Sm}$. The time-domain expression of the output voltage $v_4(t,\boldsymbol{\xi})$ is then obtained as a linear superposition of harmonics:

TABLE IV
SOURCES OF VARIATION FOR THE EXAMPLE BUNDLE OF FIG. 1.

Variable	Type	Mean value	Relative standard deviation
metallic conductors n_c	Gauss.	rN_c=169(1/3) ≈ 56.3	$\frac{\sqrt{rN_c(1-r)}}{rN_c}$ $\approx 11\,\%$
height h	Gauss.	100 nm	11 %
nanotube diameter d	Gauss.	1 nm	17 %

$$\begin{aligned} v_4(t,\boldsymbol{\xi}) = \bar{v}_4 + \textstyle\sum_{m=1}^{M} \big[V_4(j2\pi f_m,\boldsymbol{\xi})\mathrm{e}^{j2\pi f_m t} + \\ + V_4^*(j2\pi f_m,\boldsymbol{\xi})\mathrm{e}^{-j2\pi f_n t}\big], \end{aligned} \tag{21}$$

where $\bar{v}_4$ is the DC term, obtained from a DC calculation, and the output coefficients $V_4(j2\pi f_n,\boldsymbol{\xi})$ are computed according to (19). The linearity of Fourier decomposition assures that the PC structure is preserved also for the time-domain expression of the output:

$$\begin{aligned} v_4(t,\boldsymbol{\xi}) = \bar{v}_4 + v_{4,0}(t)\phi_0(\boldsymbol{\xi}) + v_{4,1}(t)\phi_1(\boldsymbol{\xi}) + \\ + v_{4,2}(t)\phi_2(\boldsymbol{\xi}) + v_{4,3}(t)\phi_3(\boldsymbol{\xi}), \end{aligned} \tag{22}$$

where

$$\begin{aligned} v_{4,j}(t) \;=\; \textstyle\sum_{m=1}^{M} \big[V_{4,j}(j2\pi f_m)\mathrm{e}^{j2\pi f_m t} + \\ + V_{4,j}^*(j2\pi f_m)\mathrm{e}^{-j2\pi f_m t}\big] \end{aligned} \tag{23}$$

with $j = 0, 3$. This is the expression that is used in practice for the numerical validation in the next section.

E. Application to the Multiconductor Case

The application of the aforementioned steps to the multiconductor circuit of Fig. 3 is straightforward, since PC is not limited to single-conductor lines, as shown in [20]. Specifically, the transmission matrices $\mathbf{T}_1$ and $\mathbf{T}_3$ become block matrices, where each block is diagonal and has a size of $n_c \times n_c$. The expansion of each block is similar to (12) but with coefficients made of matrices, filling the augmented matrix blocks as shown in (16). As far as the transmission line augmented matrix $\tilde{\mathbf{T}}_2$ is concerned, it can be computed with the same procedure outlined in Sec. V-B.

VI. NUMERICAL RESULTS

In this Section, the proposed technique is applied to the analysis of the test structure of Fig. 4, that describes a $\mathcal{L}$=100 μm long SWCNT bundle placed over a ground plane. A SWCNT is chosen for the stochastic analysis since it is based on the information in reference [14], that provides a

detailed description of process variations with realistic values. Moreover, the ESC model is used, since it is simpler and does not require a numerical evaluation of the classical p.u.l. parameters. On the other hand, a validation of the ESC model and its comparison with the full MTL model is out of the scope of this paper and readers are referred to [7] and [10].

As already outlined in the previous Section, the driver of Fig. 4 is replaced by a Thevenin equivalent with a series impedance $Z_S = 25\,\Omega$. Similarly, the receiver is replaced by the impedance $Z_L = 1/sC_L$, with $C_L = 10^{-2}$ pF. The variability is provided by the number n_c of conducting tubes, the height h of the bundle above the ground plane and the diameter d of the single nanotube (see eq. (9) and Table IV, that summarizes the coefficients defined in agreement with [14]). According to (7), the bundle radius R_b turns out to be 9.88 nm.

The approximate relations of Sec. V, are used to compute the PC expansion of the unknowns and of the parameters of the structure leading to (15) and (17).

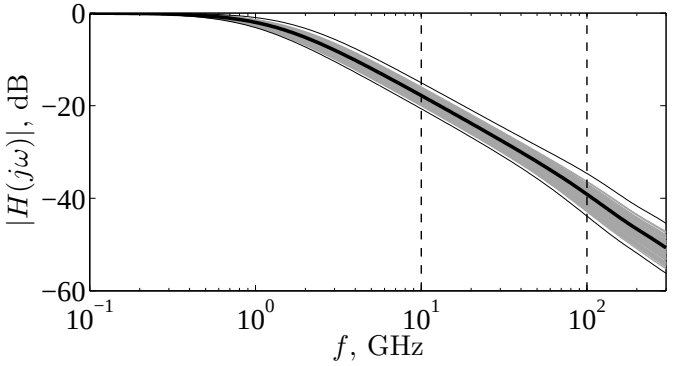

Fig. 6. Bode plots (magnitude) of the transfer function $H(j\omega)$=$V_4(j\omega)/E(j\omega)$ of the example test case of this study (see text for details). Solid black thick line: deterministic response; solid black thin lines: 3-σ tolerance limit of the second-order polynomial chaos expansion; gray lines: a sample of responses obtained by means of the MC method (limited to 100 curves, for graph readability).

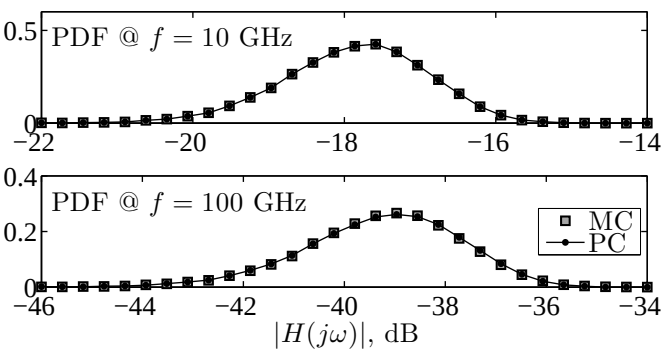

Fig. 7. Probability density function of $|H(j\omega)|$ computed for two different frequencies. The distributions marked MC refer to 40,000 MC simulations, and those marked PC refer to the response obtained via second-order polynomial chaos expansion.

Figure 6 shows a comparison of the Bode plot (magnitude) of the transfer function $H(j\omega) = V_4(j\omega)/E(j\omega)$ computed via the advocated PC method and determined via a number of MC simulations. In order to provide a quantitative statistical information on the variability effects of system responses, Fig. 7 compares the PDF of $|H(j\omega)|$ computed for different frequencies over a large number (40,000 in this case) MC simulations, and the distribution obtained form the analytical PC expansion of $H(j\omega)$. The frequencies selected for this comparison correspond to the vertical dashed lines shown in Fig. 6. The good agreement between the actual and the predicted PDFs and, in particular, the accuracy in reproducing the tails and the large variability of non-Gaussian shapes of the reference distributions, confirm the potential of the proposed method. For this example, it is also clear that a PC expansion with a very limited number of terms is accurate enough to capture the dominant statistical information of the frequency-domain system response.

In addition, Fig. 8 shows the surface of $|H(j\omega)|$ computed at f=100 GHz as a function of the variability parameters, for two values of the PC expansion order p. To avoid multidimensional plots and improve readability, the three-dimensional plot shown in the Figure is a function of the two random variables only, i.e., ξ_1 and ξ_2, for the nominal value of ξ_3 (see eq. (9)). Similar results can be obtained with different cuts of the multidimensional surface. The above plot highlights that the third order expansion is sufficient for the approximation of the actual multidimensional surface for a wide range of parameter variability.

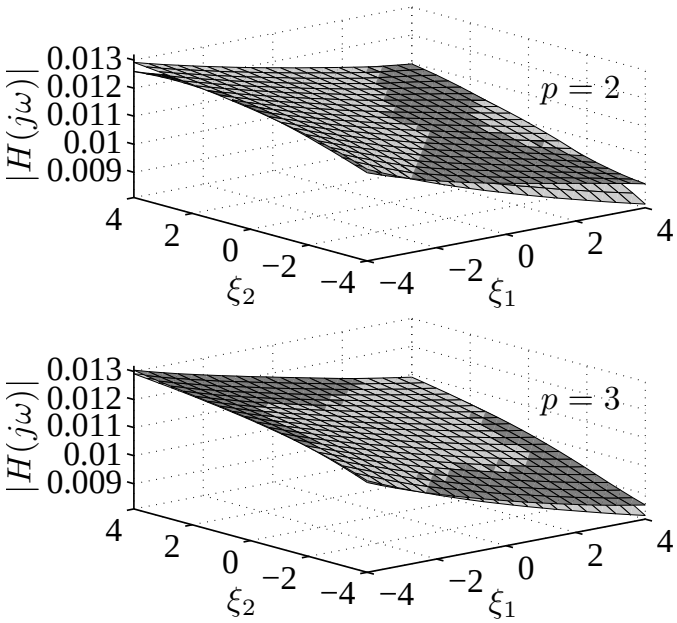

Fig. 8. Plot of $|H(j\omega)|$ at f=100 GHz as a function of the random parameters ξ_1 and ξ_2 (see eq. (9)) and two different orders of the PC expansion (see text for details). The surfaces are obtained by setting ξ_3=0, that corresponds to the nominal value of the nanotube diameter d. Light gray: reference; dark gray: PC approximations.

Figure 9 collects similar results for the transient analysis of the example nanointerconnect. The Figure shows the time-domain response of the voltage $v_4(t)$ and its PDF computed according to the procedure of Sec. V. The Thevenin voltage

source mimics a digital driver producing a trapezoidal signal with $\tau = 3\,\text{ps}$ rise time and a period of $2\,\text{ns}$. To compute the Fourier series of the source $e_S(t)$, according to (20), a number 200 of harmonics is considered.

In order to further validate the proposed method, Fig. 10 collects the time-domain response of the example nanointerconnect with a different set of parameters. In particular, the values of the line length $\mathcal{L}$, the load capacitance C_L and the rise time τ are further reduced (i.e., $\mathcal{L}$=20 μm, $\tau = 0.3\,\text{ps}$ and $C_L = 10^{-4}\,\text{pF}$). In this second time-domain validation, the period of the voltage source $e_S(t)$ is set to 20 ps and 50 harmonics are considered to compute its Fourier series expansion. Admittedly, the above parameters values are somewhat extreme, but have been chosen in order to stress the method and assess its performance for the prediction of the variability of a response corrupted by the line reflections.

With the above time-domain comparisons and the good agreement between the PDFs obtained from the PC model and the corresponding set of MC simulations, the potential of the proposed method is clearly confirmed, as already highlighted for the frequency-domain analysis.

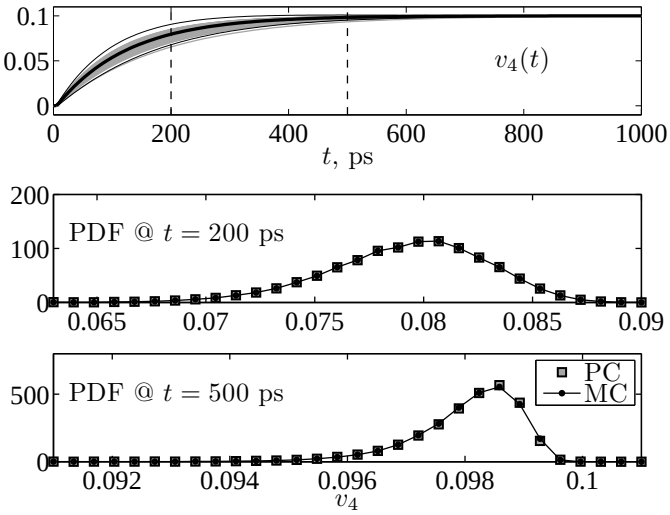

Fig. 9. Top panel: transient response $v_4(t)$ for the nanointerconnect of this study, with $\mathcal{L}$=100 μm, τ=3 ps and C_L=10^{-2} pF. Solid black thick line: deterministic response; solid black thin lines: 3-σ limits of the third-order PC expansion; gray lines: a sample of responses obtained by means of the MC method (limited to 100 curves, for graph readability). Bottom panels: probability density function of the near-end crosstalk $v_4(t)$ computed at different times. Of the two distributions, the one marked MC refers to 40,000 MC simulations, while the one marked PC refers to the response obtained via the PC expansion

As far as the efficiency is concerned, it is relevant to remark that the proposed PC method is faster by two orders of magnitude with respect to the MC approach in computing the probability functions of Fig. 7 (see Tab. V). This holds even if for fairness we consider the computational overhead required by the creation of the augmented set of equations (15) and (17).

In summary, the proposed method allows to generate accurate predictions of the statistical behavior of a realistic nanointerconnect with a great efficiency improvement. Moreover, it offers an interesting and promising alternative to other

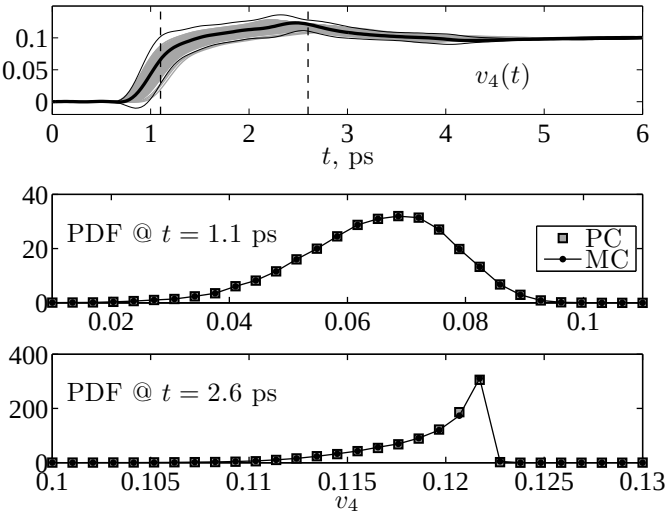

Fig. 10. Transient response $v_4(t)$ for the nanointerconnect of this study (top panel) and its PDF (bottom panel). The curves in this figure are computed with $\mathcal{L} = 20\,\mu$m, τ=0.3 ps and C_L=10^{-4} pF. The same notation of Fig. 9 applies here.

TABLE V
CPU TIME REQUIRED BY THE COMPUTATION OF THE CURVES OF FIG. 7 BY MEANS OF THE MC AND OF THE PROPOSED PC-BASED METHODS.

Method	Order p	Overhead	Simulation time
MC	–	–	44 min
PC	2	4.5 sec	7.8 sec
PC	3	5.3 sec	8.7 sec

stochastic methods such as Stochastic Collocation Method (SCM) [23]. Perhaps, the most appealing feature is that PC provides a single stand-alone model that inherently includes the effects of variability instead of being somewhat based on the processing of a set of system responses (e.g., their interpolation in the case of SCM). This means that the model is generated only once and it can be used for the simulation of realistic structures with possibly different source and load conditions as well as integrated into more complex circuits, without the need of recomputing the model coefficients. Furthermore, it belongs to the same class as the original one and thus it can be solved using the same deterministic procedure or solver. Finally, the magnification of the system complexity is probably smaller in PC than in SCM, although unlike SCM the resulting PC model is fully coupled and this suggests that a trade-off between these two methods exists according to the number of random variables and order of accuracy.

VII. CONCLUSIONS

This paper deals with the generation of an enhanced model for the stochastic analysis of a CNT interconnect structure that includes the effects of process variation. The proposed approach is based on the available state-of-the-art deterministic models of a nanointerconnect that are expressed via an equivalent transmission-line formulation. The governing electrical

laws of the adopted models turn out to contain uncertain parameters related to geometrical or material properties of the structure, that can be considered as random quantities. Polynomial chaos theory is then employed to address the stochasticity of the problem. This procedure, by means of an Hermite polynomials expansion of the structure parameters and of the electrical unknowns, leads to an extended set of equations belonging to the same class of the deterministic ones. The solution of such equations provides a quantitative prediction of the statistical information of the parameters variability effects on the interconnect response.

The strengths of the approach expressed in terms of both accuracy and efficiency has been demonstrated via the frequency- and time-domain analysis of a realistic nanointerconnect with three uncertain parameters. Although further investigations are worth to be considered for highlighting the impact of process variations on nanotube interconnects via the proposed methodology, they are planned as a next step and therefore out of the scope of this paper, that is limited to the model derivation.

REFERENCES

[1] V. N. Popov, "Carbon Nanotubes: Properties and Application," *J. Materials Science and Engineering*, Vol. 43, No. 3, pp. 61–102, Jan. 2004.

[2] S. Salahuddin, M. Lundstrom and S. Datta, "Transport Effects on Signal Propagation in Quantum Wires," *IEEE Trans. Electron Devices*, Vol. 52, No. 8, pp. 1734–1742, Aug. 2005.

[3] G. F. Close and H. S. P. Wong, "Assembly and Electrical Characterization of Multiwall Carbon Nanotube Interconnects," *IEEE Trans. Nanotechnology*, Vol. 7, No. 5, pp. 596–600, Sep. 2008.

[4] A. Maffucci, "Carbon Nanotubes in Nanopackaging Applications," *IEEE Nanotechnology Magazine*, Vol. 3 , No. 3, pp. 22–25, 2009.

[5] H. Li, C. Xu, and K.Banerjee, "Carbon Nanomaterials: The Ideal Interconnect Technology for Next-Generation ICs", *IEEE Design & Test of Computers*, pp. 20–31, 2010.

[6] M. S. Sarto and A. Tamburrano, "Electromagnetic Analysis of Radio-Frequency Signal Propagation Along SWCN Bundles," Proc. of *6th IEEE Int. Symp. NANO*, Cincinnati, OH, pp. 201-204, Jul. 17-20, 2006.

[7] M. S. Sarto and A. Tamburrano, "Single-Conductor Transmission-Line Model of Multiwall Carbon Nanotubes," *IEEE Trans. Nanotechnology*, Vol. 9, No. 1, pp. 82–92, Jan. 2010.

[8] M. D'Amore, M. S. Sarto and A. Tamburrano, "Fast Transient Analysis of Next-Generation Interconnects Based on Carbon Nanotubes," *IEEE Trans. Electromagnetic Compatibility*, Vol. 52, No. 2, pp. 496–503, May 2010.

[9] H. Li, W Yin, K. Banerjee, and J. Mao "Circuit Modeling and Performance Analysis of Multi-Walled Carbon Nanotube Interconnects," *IEEE Trans. Electron Devices*, Vol. 55, No. 6, pp. 1328–1337, Jun. 2008.

[10] M. D'Amore, M. Ricci and A. Tamburrano, "Equivalent Single Conductor Modeling of Carbon Nanotube Bundles for Transient Analysis of High-Speed Interconnects," Proc. of *8th IEEE Int. Symp. NANO*, Arlington, TX, pp. 307-310, Aug. 18-21, 2008.

[11] M. S. Sarto and A. Tamburrano, "Multiconductor Transmission Line Modeling of SWCNT Bundles in Common-Mode Excitation," Proc. of *6th IEEE Int. Symp. EMC*, Portland, OR, pp. 466-471, Aug. 14-18, 2006.

[12] C. R. Paul, *Analysis of Multiconductor Transmission Lines,* Wiley, 1994.

[13] Y. Massoud and A. Nieuwoudt, "Modeling and Design Challenges and Solutions for Carbon Nanotube-Based Interconnect in Future High Performance Integrated Circuits," *ACM J. Emerg. Technol. Comput. Syst.*, Vol. 2, No. 3, pp. 155–196, Jul. 2006.

[14] A. Nieuwoudt and Y. Massoud, "On the Impact of Process Variations for Carbon Nanotube Bundles for VLSI Interconnect," *IEEE Trans. Electron Devices*, Vol. 54, No. 3, pp. 446–455, Mar. 2007.

[15] A. Nieuwoudt and Y. Massoud, "On the Optimal Design, Performance, and Reliability of Future Carbon Nanotube-Based Interconnect Solutions," *IEEE Trans. Electron Devices*, Vol. 55, No. 8, pp. 2097–2110, Aug. 2008.

[16] N. Wiener, "The Homogeneous Chaos", *Amer. J. Math.*, Vol. 60, pp. 897–936, 1938.

[17] D. Xiu and G. E. Karniadakis, "The Wiener-Askey Polynomial Chaos for Stochastic Differential Equations," *SIAM, Journal of Sci. Computation*, Vol. 24, No. 2, pp. 619–622, 2002.

[18] K. Strunz and Q. Su, "Stochastic Formulation of SPICE-Type Electronic Circuit Simulation with Polynomial Chaos," *ACM Tran. Modeling and Computer Simulation*, Vol. 18, No. 4, pp. 15:1–15:23, Sep. 2008.

[19] P. Manfredi, I. S. Stievano and F. G. Canavero, "Parameters Variability Effects on Microstrip Interconnects via Hermite Polynomial Chaos," Proc. of the *19th IEEE Conference on Electrical Performance of Electronic Packaging and Systems, EPEPS*, Austin, TX, pp. 149–152, Oct. 25–27, 2010.

[20] I. S. Stievano, P. Manfredi and F. G. Canavero, "Parameters Variability Effects on Multiconductor Interconnects via Hermite Polynomial Chaos," *IEEE Trans. Components, Packaging and Manufacturing Technology*, Vol. 1, No. 8, pp. 1234–1239, Aug. 2011.

[21] Y. Li, S. Peng et Al., "On the Origin of Preferential Growth of Semiconducting Single-Walled Carbon Nanotubes", *J. Phys. Chem. B 109*, pp. 6968–6971, Apr. 2005.

[22] I. S. Stievano, F. Canavero, "Response Variability of High-Speed Interconnects via Hermite Polynomial Chaos," Proc. of *14th IEEE Workshop on Signal Propagation on Interconnects*, Hildesheim, Germany, pp. 3–6, May 9–12, 2010.

[23] I. Babuška, F. Nobile, R. Tempone, "A Stochastic Collocation Method for Elliptic Partial Differential Equations with Random Input Data," *SIAM J. Numer. Anal.*, Vol. 45, No. 3, pp. 1005–1034, May 2007.